

ARTICLE TYPE

Heterogeneous Clinical Trial Outcomes via Multi-Output Gaussian Processes

Owen Thomas*¹ | Leiv Rønneberg²¹HØKH, Akershus University Hospital, Lørenskog, Norway²MRC Biostatistics Unit, University of Cambridge, Cambridge, UK**Correspondence**

*Email: owen.thomas@ahus.no

Summary

We make use of Kronecker structure for scaling Gaussian Process models to large-scale, heterogeneous, clinical data sets. Repeated measures, commonly performed in clinical research, facilitate computational acceleration for nonlinear Bayesian non-parametric models and enable exact sampling for non-conjugate inference, when combinations of continuous and discrete endpoints are observed. Model inference is performed in Stan, and comparisons are made with brms on simulated data and two real clinical data sets, following a radiological image quality theme. Scalable Gaussian Process models compare favourably with parametric models on real data sets with 17,460 observations. Different GP model specifications are explored, with components analogous to random effects, and their theoretical properties are described.

KEYWORDS:

Gaussian Processes, Scalable Inference, Repeated Measures, Kronecker Products, Heterogeneous Multi-output Regression, Stan, Radiological Image Quality

1 | INTRODUCTION

Clinical research is often performed with structured data built into the study design, sometimes by repeated measurements of individuals at different time points or locations, or using different measurements methods simultaneously on the same individuals. For example, longitudinal studies follow the same cohort repeatedly at different points using the same measurement process, while many Randomised Control Trials (RCTs) will simultaneously measure primary and secondary endpoints reflecting different aspects of a clinical process.

In the article, we observe that either of these types of structured measurement can be used to enable computational tractability of a class of complex statistical models that would otherwise not scale to real clinical data sets of thousands of measurements. Specifically, appropriate repeated measurements enable the pursuit of exact inference for Gaussian Process (GP)² models by representing their covariance matrices as Kronecker products². GPs are Bayesian nonparametric models, that are capable of capturing nonlinear covariate dependence, or multi-output correlations² that would ordinarily be neglected by commonly-used parametric statistical models.

Here we present and run new GP models using repeated measurements in the covariate structure and multiple heterogeneous (mixed continuous and discrete) outputs: exact inference in Stan² is scaled to tens of thousands of measurements on the processors of a domestic-issue laptop. The models represent the joint covariance between all of the data as Kronecker-structured, and perform Hamiltonian Monte Carlo (HMC) sampling for hyperparameters, missing output values, and on the latent GP space for non-conjugate inference in the presence of heterogeneous outputs. The clinical data sets follow the theme of radiological image

⁰**Abbreviations:** GP, Gaussian Process; HMC, Hamiltonian Monte Carlo; RCT, Randomised Control Trial; ARD, Automatic Relevance Determination; NUTS, No U-Turn Sampler; CTA, Computed Tomography Angiography; keV, kiloelectronVolts; ROI, Region Of Interest; SVM, Support Vector Machine; ESS, Effective Sample Size; HU, Hounsfield Unit; ICM, Intrinsic Coregionalization Model

quality, in which the covariates consist of patient characteristics, body locations and time, while the outputs represent measurements of image quality, either continuously "objectively" on the Hounsfield scale² of radiodensity, or discretely "subjectively" from expert evaluations.

MAIN ARTICLE CONTRIBUTIONS

- The observation that widely-used repeated measurements in clinical research, either in the form of making the same measurement at different points, or making different measurements simultaneously, facilitates the use of Kronecker structure in the covariance matrix of Gaussian Process models and thereby the scaling of exact sampling for Bayesian nonparametric models to large clinical data sets with modest computational resources.
- An implementation of the relevant Gaussian Process models in Stan^{2,3} (with wrapper in R), allowing for running the inference on multiple real world data sets, and benchmarking various model specifications such as covariance function choices.
- An empirical investigation using real-world clinical data sets into the predictive abilities of the Gaussian Process models compared to standard parametric regression models run in brms², demonstrating the utility of more complex models.

2 | METHODS

In this section, we describe the methodological concepts relevant to the models implemented in this article.

2.1 | Repeated Measurements

The value of repeated measurements is well-established and widely-understood in clinical research. The use of random effects is common when data is drawn from a structured population for which a hierarchical model is appropriate, for example when measuring different individuals repeatedly, or in a multi-centre study. Further structure emerges if data is collected in a systematic way, for example at consistent follow-up times for the entire population, or at multiple, consistent anatomical locations in the body for scans or biopsies. Data can also exhibit repetitions at the outcome level, when different outcomes of interest are measured at the same locations, individuals, and time points: this is common in RCTs with a combination of primary and secondary endpoints.

Within a regression framework, the multiple outcomes can be represented as a matrix Y , and the covariates corresponding to treatments, locations, times, patient characteristics, or anything else that might influence the outcomes, can be represented as a covariate matrix X . Different clinical study designs will impose different structure on the covariate matrix X . If we consider a design in which N_1 individuals are measured at N_2 time points, at N_3 anatomical locations, with the time points and anatomical locations being identical between individuals, then we can divide columnwise the long-format covariate matrix X of height $N_1 N_2 N_3$ into matrices X_1 , X_2 , and X_3 , with X_1 containing information x_1 about the N_1 unique individuals, repeated $N_2 N_3$ times, X_2 containing information x_2 about the N_2 unique times of measurement, repeated $N_1 N_3$ times, and X_3 containing information x_3 about the N_3 unique anatomical locations, repeated $N_1 N_2$ times. There are in addition N_4 distinct outcomes measured for every value of X , resulting in an outcome matrix Y of size $N_1 N_2 N_3$ by N_4 .

2.2 | Gaussian Processes

Gaussian Processes (GPs) are nonlinear, Bayesian models designed for flexible, probabilistic supervised learning². They model a dependent variable y conditional on independent variables X , via a mean function $m(x)$ and covariance¹ function $k(x, x', \theta)$,

¹also known as kernel function

defining a latent variable f that is joint-normally distributed over all the observed data points. The covariance functions are described by hyperparameters θ that can be learned from data, while the mean function will be taken to be zero here with no loss of generality. The latent function f can be passed through a Gaussian likelihood with a noise variance σ^2 to model a continuous output y :

$$f \sim \mathcal{GP}(0, k(x, x', \theta)) \quad (1)$$

$$y|x = f(x) + \epsilon, \quad \epsilon \sim \mathcal{N}(0, \sigma^2) \quad (2)$$

$$(3)$$

Specific choices of covariance functions $k(x, x', \theta)$ have corresponding implicit parametric basis functions. One advantage of the "function-space" formulation is the ability to use a finite representation of a function with a potentially infinite-dimensional parametric representation: this is the sense in which the models are considered "nonparametric", in that they avoid specifying a parametric model for the latent mean function.

2.3 | Scalability and Kronecker-Structure Covariance Matrices

Asserting a GP with a covariance function $k(x, x', \theta)$ over a data set with N covariate observations defines a $N \times N$ covariance² matrix \mathbf{K} , where the matrix element $\mathbf{K}[i, j]$ is equal to the covariance function $k(x^i, x^{j'}, \theta)$ evaluated at the i th and j th data point. One challenge of working with GPs is the need to perform a decomposition of the $N \times N$ covariance matrix, which is the dominant computational demand when evaluating the marginal likelihood for sampling or computing the predictive distributions. This results in $\mathcal{O}(N^3)$ cubic scaling in computational costs with the number of data points N , ruling out exact inference for generic covariance matrices for larger data sets. Various methods exist to enable *approximate inference* for larger data sets^{2,3}, while exact inference is possible for larger data sets when there is structure in the covariance matrix that can be exploited, such as Kronecker or Toeplitz². In instances where data can be represented as lying in a grid structure, with separable covariance structure between each dimension of the grid, the full covariance matrix can be represented as a Kronecker product between the dimensions. A Kronecker product is an operation performed on two matrices generating a third matrix composed of each individual element of the first matrix separately multiplied with the entire second matrix, combined in a blockwise fashion, i.e. for two matrices A and B :

$$\mathbf{A} \otimes \mathbf{B} = \begin{bmatrix} a_{11}\mathbf{B} & \cdots & a_{1n}\mathbf{B} \\ \vdots & \ddots & \vdots \\ a_{n1}\mathbf{B} & \cdots & a_{nn}\mathbf{B} \end{bmatrix} \quad (4)$$

For a data set consisting of covariates measured over a two dimensional grid, for example the pixels of an image, the covariance matrix over the entire data set ($\mathbf{K}_{12} = K([x_1, x_2], [x'_1, x'_2])$) can be represented as the Kronecker product between two covariance matrices representing each grid dimension independently ($\mathbf{K}_1 = K(x_1, x'_1)$, $\mathbf{K}_2 = K(x_2, x'_2)$), with the constraint that the covariance functions used are separable, i.e. for a grid composed of n_1 vertical grid points x_1 , and n_2 horizontal grid points x_2 , then:

$$\mathbf{K}_{12} = \mathbf{K}_1 \otimes \mathbf{K}_2. \quad (5)$$

We can apply this reasoning to clinical scenario described in 2.1: for a longitudinal study consisting of N_1 individuals measured at N_2 time points at N_3 anatomical locations, the covariate data X can be represented as lying on a three dimensional grid, where one of the grid dimensions x_1 is the variation between individuals, the second x_2 as the variation in time, and the third x_3 variation in anatomical location. Consequently, defining separate covariance matrices representing the variation across individuals (the $N_1 \times N_1$ matrix \mathbf{K}_1), variation over time (the $N_2 \times N_2$ matrix \mathbf{K}_2), and anatomical variation (the $N_3 \times N_3$ matrix \mathbf{K}_3) we can represent the covariance between the covariate measurements X as:

$$\mathbf{K}_X = \mathbf{K}_1 \otimes \mathbf{K}_2 \otimes \mathbf{K}_3. \quad (6)$$

Conveniently, when a decomposition of the full matrix is required, the components of the Kronecker product can be decomposed separately, such that the $\mathcal{O}(N^3) = \mathcal{O}(N_1^3 N_2^3 N_3^3)$ computational demands become $\mathcal{O}(N_1^3 + N_2^3 + N_3^3)$. For datasets with

²also known as kernel matrix

appropriate grid structure or repeated measurements, this enables exact inference for tens of thousands of data points on a personal computer. This has been used previously for image data, where the pixels lie on a regularly spaced grid, or when there are multiple endpoints evaluated at the same covariate locations. In this article, we note that the widespread use of repeated measurements in clinical research, can be represented within the Kronecker structure described above.

2.4 | Heterogeneous Multi-Task Gaussian Processes

The GP framework extends naturally to multi-dimensional responses \mathbf{Y} , analogous to the case of multivariate regression²². The different response dimensions (also known as "tasks" or "outputs") are appended into a single vector, and a between-task covariance matrix \mathbf{K}_{out} is used to model correlations between the tasks. When the different tasks are evaluated at the same values of the covariates, generating a covariance matrix between covariates \mathbf{K}_X then Kronecker structure again emerges in the full covariance matrix $\mathbf{K}_f = \mathbf{K}_{out} \otimes \mathbf{K}_X$, and computational accelerations become possible.

Different tasks often correspond to different methods of evaluating some outcome, and often exhibit heterogeneity of distributions, e.g. each task may be variously continuous valued, binary or follow some other distribution. In this case, each output will require different likelihood functions to map from the latent function f to observation y . For likelihoods other than Gaussian, the latent variable cannot be integrated out analytically and inference must be performed for the latent variable, through sampling, variational inference, or another approximation.

All of the data sets used in this article use one Kronecker component for the multi-output correlation, and three Kronecker grid components for the covariates, which are grouped into grid dimensions x_1 , x_2 and x_3 . The full covariance structure is therefore:

$$\mathbf{K}_f = \mathbf{K}_{out} \otimes \mathbf{K}_1 \otimes \mathbf{K}_2 \otimes \mathbf{K}_3 \quad (7)$$

2.5 | Covariance Matrix Design and Random Effects

Imposing Kronecker structure on the full covariance matrix puts some constraints on the types of covariance functions that can be used. Principally, the covariance function must be separable between the different grid components x_1 and x_2 , meaning the overall covariance function can be represented as the product of covariance functions defined over of the grid components, i.e. $k([x_1, x_2], [x'_1, x'_2]) = k_1(x_1, x'_1)k_2(x_2, x'_2)$. Many commonly used multi-dimensional covariance functions exhibit this property, but some designs that might be desirable for interpretation do not exhibit separability. Two are discussed below: additive covariance functions and random effects covariance functions.

An additive covariance function represents a common covariance function over different dimensions as a sum of separate covariance functions², i.e. $k([x_1, x_2], [x'_1, x'_2]) = k_1(x_1, x'_1) + k_2(x_2, x'_2)$. Additive covariance functions might be desired if we are interested in isolating the particular contribution to the output variation from one particular dimension. This is especially useful in medical research when one intervention or treatment is considered to be of central clinical relevance. Within the Kronecker framework, it is possible to assert an additive covariance function within each component of the Kronecker product, but the resulting covariance function over the entire data set is a product of the sum within the component with the covariance functions over the rest of the dimensions, making it different to interpret the sum components separately, i.e.:

$$(\mathbf{K}_1 + \mathbf{K}_2) \otimes \mathbf{K}_3 = (\mathbf{K}_1 \otimes \mathbf{K}_3) + (\mathbf{K}_2 \otimes \mathbf{K}_3) \quad (8)$$

Random effects are often desirable in the presence of repeated measurements, where we are not necessarily interested in the variation between individuals but we would still like to include it in the model². This can be performed in an elegant way within GP regression models by including a structured diagonal noise component representing the random variation across individuals. In the Kronecker context, this can be achieved by adding spherical noise to the Kronecker product component that represents the variation between individuals, representing the "noise" sampled when moving between individuals. As this is an additive covariance function where one of the covariance functions is diagonal noise, the same problem emerges when combining additive covariance functions with Kronecker structure: the resulting covariance function components cannot be interpreted totally straightforwardly, as they are multiplied with the covariance functions associated with the other Kronecker components. Formally, a traditional random effects model is represented in the first half of the following inequality, and the model we implemented in the second:

$$(\mathbf{K}_1 \otimes \mathbf{K}_2) + (\sigma^2 \mathbf{I}_1 \otimes \mathbf{I}_2) \neq (\mathbf{K}_1 + \sigma^2 \mathbf{I}_1) \otimes \mathbf{K}_2 \quad (9)$$

This formulation of a random effect is equivalent to adding some extra variance to the coefficients corresponding to non-patient specific covariates. We detail this in Appendix B, for the case where all kernels are linear and thus GP regression is equivalent to Bayesian linear regression.

We ran separate models with and without the "random effect" noise in the individual-level covariance function to explore its influence on the model fit and predictions. We call the models with and without this the mixed-effect GP ("GP.m") and the fixed-effect GP ("GP.f").

The covariance functions for each covariate were chosen conditional on the data. For continuous-valued covariates, a squared-exponential covariance function with a lengthscale hyperparameter enabling automatic relevance determination (ARD) was used. For binary covariates, a linear covariance function was used with a variance hyperparameter, as a more complex covariance function would be unnecessary for binary data. Nominal or ordinal covariates were one-hot encoded to corresponding binary variables and a linear covariance function used. The multi-output covariance matrix \mathbf{K}_{out} is parametrised as a Cholesky-decomposed correlation matrix multiplied with a diagonal matrix representing the separate output variances.

2.6 | Full Model Specification

In summary, the three-component Kronecker model used in this article, with n_g Gaussian-distributed outputs y_g , n_b Bernoulli-distributed outputs y_b , and repeated covariates partitioned into repeated measure grid components x_1 , x_2 and x_3 , becomes:

$\rho_1, \rho_2, \rho_3 \sim \text{InvGamma}(2, 1)$	Lengthscales for each kernel Kronecker component
$\alpha \sim \text{InvGamma}(2, 1)$	Kernel variances for each output
$\alpha^{(n)} \sim \text{InvGamma}(2, 1)$	Noise variance for each Gaussian-distributed output
$\eta \sim \mathcal{N}(0, 1)$	Standard Normal latent η for computation purposes
$L \sim \text{LkjCholesky}(3)$	Correlation matrix between outputs with LkjCholesky prior
$L^{(n)} \sim \text{LkjCholesky}(3)$	Noise correlation matrix between Gaussian outputs with LkjCholesky prior
$\sigma_{re}^2 \sim \text{InvGamma}(2, 1)$	Variance of optional random effects kernel component
$K_1 = k(x_1, x_1, \rho_1)$	First Kronecker kernel matrix component
$K_2 = k(x_2, x_2, \rho_2)$	Second Kronecker kernel matrix component
$K_3 = k(x_3, x_3, \rho_3) + \sigma_{re}^2 \mathbf{I}$	Third Kronecker kernel matrix component, with optional random effects
$f = \text{diag}(\alpha)L \otimes \text{chol}(K_3) \otimes \text{chol}(K_2) \otimes \text{chol}(K_1)\eta$	Latent variable f constructed from kernels and η
$\Sigma^{(n)} = \text{diag}(\alpha^{(n)})L^{(n)}(\text{diag}(\alpha^{(n)})L^{(n)})^T$	Noise covariance between Gaussian-distributed outputs
$y_g \sim \mathcal{N}(f[1 : n_g,], \Sigma^{(n)})$	Distribution of n_g Gaussian-distributed outputs y_g
$y_b \sim \text{Bernoulli}(\Phi(f[n_g + 1 : n_g + n_b,]))$	Distribution of n_b Bernoulli-distributed outputs y_b

2.7 | Stan Implementation

The methods described here were implemented in Stan[?], a probabilistic programming language designed for Bayesian inference, in which model specification is performed explicitly within the language, and No U-Turn Sampler (NUTS) Hamiltonian Monte Carlo[?] (HMC) is performed for the model parameters. The Gaussian Process was represented for inference with a standardised, uncorrelated Gaussian latent variable η , which was reshaped and transformed by the covariance Kronecker components to form the latent variable f conditioned on the covariance. HMC was performed for the GP hyperparameters and noise terms, the latent function representation η , the latent function f for discrete-valued tasks, and the missing values of the outputs. The Stan programs were called from within the R programming language via Rstan[?]. Similar computational speedups have been achieved in Stan previously^{??}.

2.8 | Missing Data

In the case of missing values of the output variable y , which often arise when exploiting Kronecker structure over an incomplete grid, the Bayesian framework offers a convenient solution: the missing y values are treated as parameters to be inferred, using the distribution implied by the latent variable f and likelihood $p(y|f)$, conditional on the observed covariates. The scalability associated with the Kronecker decomposition is preserved, while interpretable posterior distributions for the unobserved data are provided.

The inference for continuous-valued missing outputs y can be integrated in a straightforward way with most inference schemes. Given that Stan cannot perform inference over discrete variables, then the missing binary outputs pose a challenge. This was resolved by calculating the log-likelihood contributions according to the Bernoulli likelihood with an appropriate link function, with the missing y varying continuously between zero and one. This allows for efficient gradient-informed inference procedures, and the interpretation of the imputed variables as probabilities.

2.9 | Radiological Image Quality

The clinical theme of this article is radiological image quality, a field in which it is common to combine continuous-valued "objective" measurements of image quality with discrete-valued "subjective" expert evaluations of image quality. This article uses two real data sets, the first of which is observational time-series data, and the second of which comes from a RCT with thorough repeated measures. In each case the effect of primary interest is the effect on the image quality of volume of contrast medium per body weight.

The first real data set was previously published as a clinical study in². The image quality was measured in venal blood vessels of 53 patients, with continuous-valued attenuation in Hounsfield Units as the objective endpoint, and binary evaluations of image quality from three different consultant radiologists as the subjective endpoints. Each patient was injected with a different quantity of contrast medium per body weight, and evaluations of the images were taken at six thirty-second interval time points after injection. Evaluations were also performed for each side of the body. Further covariates used were gender, age and tube voltage. Further clinical details can be found here. The combination of 53 patients, 4 endpoints, 7 time points and 2 body sides implies a covariance structure of size 2,968, but the use of the Kronecker product for each of these contributions means that the computations are readily tractable on a personal laptop.

The second real data set comes from a Randomised Control Trial assessing image quality in arterial blood vessels following Computed Tomography Angiography (CTA)². 210 patients were randomised to receive full versus half doses of contrast volume per body weight, with measurements repeated at 7 different locations in the body, and 3 different spectral energy levels measured in kiloelectronVolts (keV). Examples of images recorded at different body levels and energy levels are presented in Figure 1. Attenuation level and image noise recorded in selected Regions Of Interest (ROIs), each measured in Hounsfield units were used as continuous-valued "objective" outcomes, and two consultant radiologists evaluated every image on a nominal scale for image quality. Because of the very skew distribution of the nominal data, these were simplified to a binary variable of "Excellent" vs every other level, results into two binary "subjective" endpoints. Examples of the ordinal scale of subjective image quality are shown in Figure 2. Sex, age and flow speed of injection were also collected as relevant covariates. The combination of 210 patients, 4 endpoints, 7 body locations and three energy levels resulted in a data set of size $N = 17,640$ but again the Kronecker structure enabled exact inference with limited computational resources.

3 | RELATED WORK

Gaussian Processes have been used for decades under various names such as kriging or Bayesian kernel regression, and are related to the widely used Support Vector Machines (SVMs). Their use has increased in the past couple of decades with the advent of greater computational resources, and much research has occurred concerning their scalability to larger data sets under contemporary computational constraints. These methods often include variational inference schemes via the "inducing point" framework², or spectral methods to approximate the full covariance function via sampled Fourier features². The speedups possible through Kronecker structure have been used for some time, but have previously been used on structured image data², drug combinations², spatio-temporal modelling², and multi-task regression².

Heterogeneous multiple outputs have also received research focus: while multiple Gaussian-distributed outputs allow for analytical marginalisation of the latent variable, the presence of discrete or other non-Gaussian-distributed outputs forces the use of non-conjugate inference methods such as variational methods, Expectation Propagation or sampling of the latent variable. Here we opt for the latter solution, aided by the development of the Stan programming language and the underlying continuity and smoothness of all latent parameters of interest.

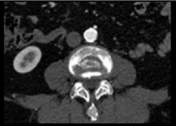
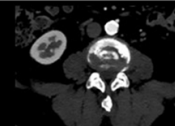
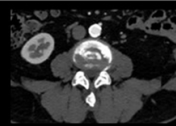
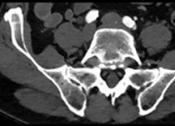
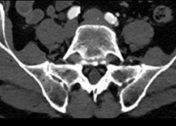
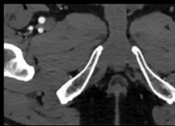
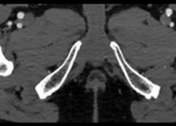
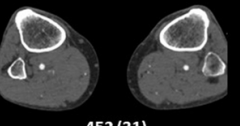
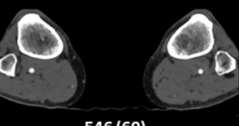
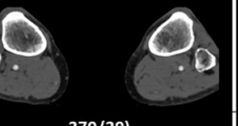
Anatomical level	Control	Experimental VMI 40 keV	Experimental VMI 50 keV	
Abdominal aorta				
Attenuation HU (SD)	417 (23)	655 (20)	438 (18)	
Common iliac artery				
Attenuation HU (SD)	420 (28)	641 (24)	427 (23)	
Superficial femoral artery				
Attenuation HU (SD)	458 (17)	570 (14)	382 (12)	
Popliteal artery				
Attenuation HU (SD)	452 (31)	546 (60)	370 (39)	

Figure 1 Lower extremity CTA in the control group and in the experimental group with energy levels at 50 and 40 keV. ROIs were placed in the abdominal aorta, common iliac artery, superficial femoral artery, and popliteal artery show attenuation and noise values. Reproduced with permission from².

4 | RESULTS

The results describing the behaviour of the trained models are presented here. We ran experiments using 10-fold cross-validation for two GP models with and without the random effect component in the individual-level covariance function ("GP.m" and "GP.f"), and two parametric models run in brms also with or without individual-level random effects ("brms.m" and "brms.f").

4.1 | Comparison in brms

Two brms models were used as comparison methods: ("brms.m" and "brms.f") with or without random effects at the individual level, respectively. Both models had linear fixed effects based on the covariates for each data set, i.e. for the simulated data example, each output modelled with the following model formulae:

```
form.yi <- yi ~ (1|p|id) + x1 + x2 + x3 # "brms.m"
form.yi <- yi ~ x1 + x2 + x3 # "brms.f"
```

with p being shared between the outputs. Either Gaussian or Binomial likelihoods were then added to the bf objects, and all outputs were learned jointly in a single call to brm. Code is available in the supplementary material.

For the first real data set, an interaction was included between time and contrast volume per unit body mass, and for the second real data set, an interaction was included between randomisation group and energy level.

4.2 | Data Simulation

Two distinct latent parametric functions were used to simulate the data, providing a nonlinear relationship between the outputs and the covariates:

$$f_1 = \exp(.15x_1) - .6x_2^2 + \sin(3x_3) \quad (10)$$

$$f_2 = -\exp(-.15x_1) + |3x_2| - \cos(3x_3) \quad (11)$$

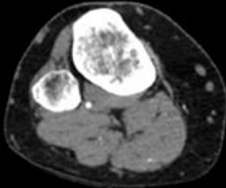
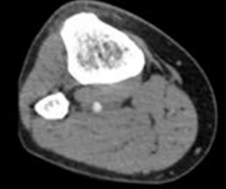
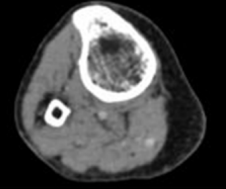
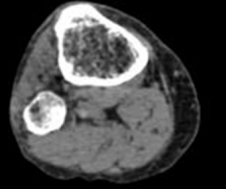
Likert scale rating	Images from the right popliteal artery
1: Excellent	
2: Good	
3: Adequate	
4: Non-diagnostic	

Figure 2 Examples of ordinal scale for subjective examination quality. Reproduced with permission from[?].

Two further latent functions were defined for the binomial outputs: $f_3 = -f_1$ and $f_4 = f_2$. All four of the latent functions then had Gaussian noise of mean zero and standard deviation 0.1 added: the resulting noisy samples for the first two outputs became the observed continuous variables, while the final two noisy samples were pushed through a probit link function and rounded to generate the observed binomial variables. No random effects were included in the data simulation process.

The covariates were sampled from $\mathcal{U}_{[-5,5]}$. 20 unique grid points were sampled for x_1 , 7 for x_2 , and 3 for x_3 . Combined with the four outputs and the Kronecker structure, this resulted in a total number of 1,680 unique observations.

The statistical models that included random effects at the individual level ("GP.m" and "brms.m") treated the third covariate x_3 as representing a measurement at the individual-level data, for the sake of comparison, but this choice is not expected to have a large influence on the results, as there was no variation in the simulated data beyond the observed covariates and shared noise.

4.3 | Losses and Testing

The models were evaluated using 10-fold cross-validation to predict the test outputs given the training data and test covariates. Loss functions were evaluated using the mean predictive f_{pm} across posterior samples and the observed data, using an absolute/L1 loss for Gaussian outputs y_g and for binomial outputs y_b , the logarithm of one minus the probability of the observed data ("the log probability of the wrong answer"), i.e. $l(y_g, f_{pm}) = |y_g - f_{pm}|$ and $l(y_b, f_{pm}) = \log(\Phi(-f_{pm} * (2y_b - 1)))$, where Φ is the probit link.

This resulted in distinct populations of losses per method, with one evaluated loss per output data point. These are plotted as histograms for each output in Figures 3, 4, 5, with the binomial losses represented on the log scale as well as the probability scale. The differences between populations of losses for each output were tested formally using a paired Wilcoxon rank sum

		GAUSSIAN				BINOMIAL			
		GP.m	brms.f	brms.m	GP.f	GP.m	brms.f	brms.m	GP.f
1	GP.m	-	-1.000	-1.000	-0.102	-	-0.778	-0.778	0.077
	brms.f	<.001	-	0.062	1.000	<.001	-	-0.005	0.769
	brms.m	<.001	0.439	-	1.000	<.001	0.953	-	0.769
	GP.f	0.405	<.001	0.000	-	0.664	<.001	<.001	-
2	GP.m	-	-0.567	-0.567	0.588	-	-0.083	0.251	-0.074
	brms.f	<.001	-	0.084	0.790	0.892	-	0.598	0.018
	brms.m	<.001	0.291	-	0.794	0.008	<.001	-	-0.196
	GP.f	<.001	<.001	<.001	-	0.892	0.892	0.055	-

Table 1 Results for the simulated data example, comparing between populations of losses for each modelling method, with the first Gaussian output in the upper left, the first Binomial to the upper right, the second Gaussian to the lower left, and the second Binomial to the lower right. Within each square, the left-lower-triangular results are the p-values from each wilcoxon rank sum test, while the right-upper-triangular results are the rank-biserial correlations representing effect sizes.

test, corrected for four-fold multiple testing degeneracy between methods. The p-values from the Wilcoxon tests were further supplemented by rank-biserial correlations as effect sizes. Nonparametric tests were chosen for model evaluation in order to avoid making distributional assumptions about the populations of losses, and to make the results robust to monotonic transformations in the losses.

For each of the four models on each of the data sets, we present posterior summaries of the interpretable model parameters from the first of the ten CV folds in tables A1 to A12. Considering the size of the data sets and the randomisation process used, we consider posterior summaries of a single CV fold to be representative of the population as a whole.

4.4 | Results for Simulated Data

We see the predictive loss results in Table 1 and Figure 3. We see that the brms model effectively fails and returns samples from the prior on binomial output 1 and Gaussian output 1, which are derived from the same latent parametric function. The GP models consequently registered significantly lower losses with large effect sizes. We see a small and possibly spurious effect of the GP models appearing to not predict around the prior at $p = 0.5$. For the second continuous output, we again see the GP models outperforming the brms models, with the GP.f performing substantially better than GP.m. For the second binomial output, we see that the brms models get many of the labels correct with high confidence, but also many of the labels wrong with high confidence. Consequently, the results here are more mixed, with the only significant differences being brms.m outperforming both GP.m and brms.f. We would expect from the absolute value present in 11 that the smooth GP model would find the second and fourth endpoints more challenging to model accurately.

Parameter posterior summaries are presented for all four models trained on this data set in tables A1 to A4.

4.5 | Observational Time-Series Data

We see the predictive loss results for the first real data set in Table 2 and Figure 4. We see that all of the methods were confidently correct in their predictions of labels for the binomial outputs, suggesting that this is a relatively easy classification problem. That said, when considering the ranking of the predictions, we see that GP.m model outperforms the other methods on the binomial outputs. We see a small number of extremely confident predictions from the brms model, especially for output 3, which is a concern even if they are correct.

When considering the continuous output, we see more mixed results between the methods, with the only clearly significant result being that the GP.f model appears to perform uniformly worse than the other methods.

Parameter posterior summaries are presented for all four models trained on this data set in tables A5 to A8.

4.6 | Randomised Control Trial Data

We see the predictive loss results for the second real data set in Table 3 and Figure 5. We again see that all four of the methods predict the correct label confidently most of the time, again suggesting that this is a relatively easy prediction problem. The brms.f method appears to return a small number of predictions from the prior for the second binomial output. We see from the hypothesis testing that the GP.m model outperforms the other three methods for the first binomial output (with a small effect size relative to GP.f), whereas the GP.f model outperforms the other methods for the second binomial output.

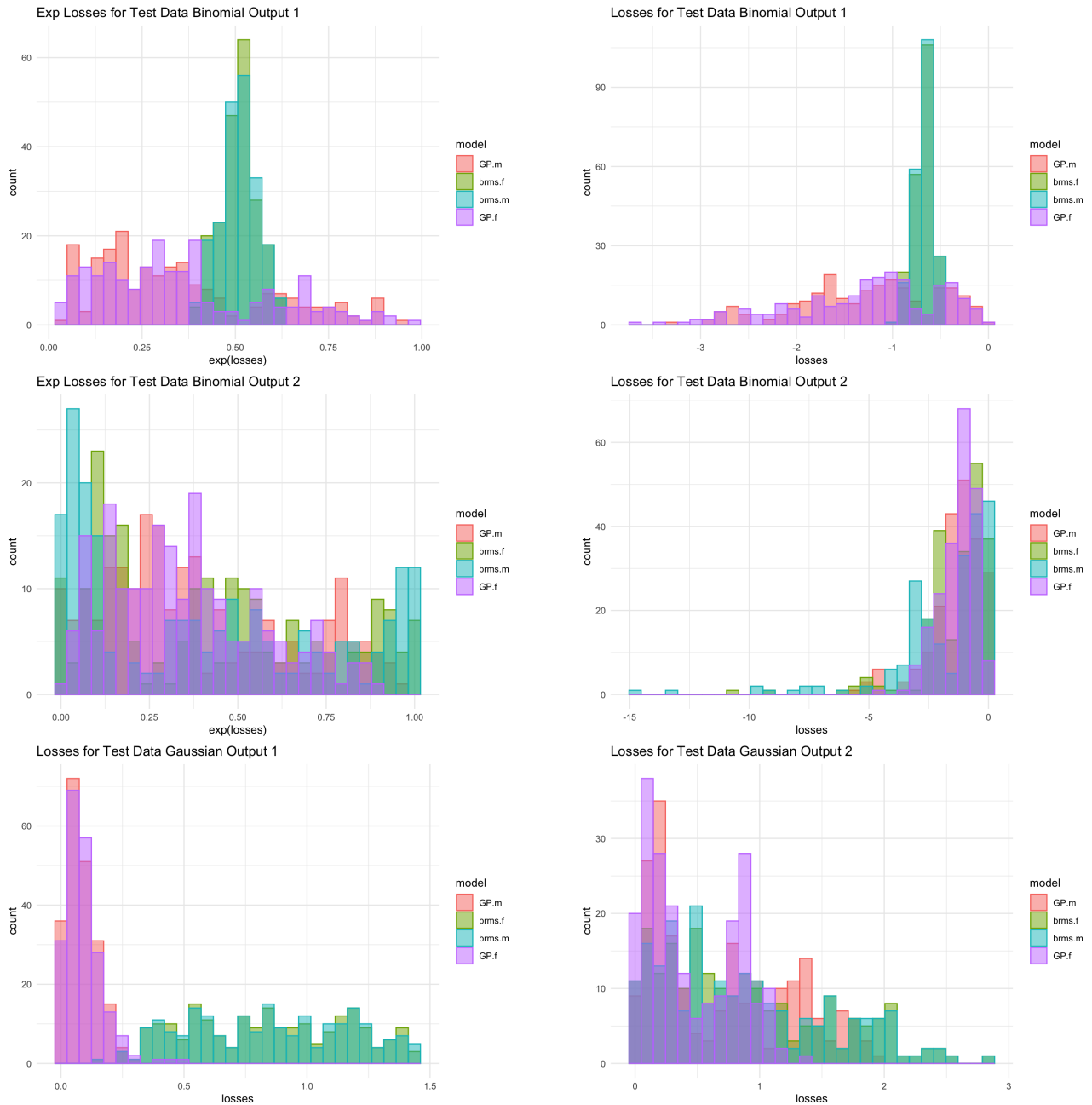


Figure 3 Figures for the simulated data example, representing histograms of losses for each of the method for each of the outputs. The uppermost two plots represent the losses on the two Gaussian-distributed outputs. Binomial outputs are plotted in the lower two rows, with those on the left on the exponentiated probability scale, and those on the right the same results plotted on the original logarithmic scale.

		GP.m	brms.f	brms.m	GP.f	GP.m	brms.f	brms.m	GP.f		
G.1	GP.m	-	0.057	0.064	-0.359	-	-0.530	-0.435	-0.839	GP.m	B.2
	brms.f	0.356	-	0.134	-0.405	<.001	-	0.840	-0.061	brms.f	
	brms.m	0.356	0.015	-	-0.408	<.001	<.001	-	-0.442	brms.m	
	GP.f	<.001	<.001	<.001	-	<.001	0.200	<.001	-	GP.f	
B.1	GP.m	-	-0.941	-0.687	-0.750	-	-0.482	-0.176	-0.879	GP.m	B.3
	brms.f	<.001	-	0.955	0.390	0.000	-	0.987	-0.010	brms.f	
	brms.m	<.001	0.000	-	-0.098	0.000	<.001	-	-0.686	brms.m	
	GP.f	<.001	<.001	0.038	-	<.001	0.835	<.001	-	GP.f	

Table 2 Results for the observational time series data set, comparing between populations of losses for each modelling method, with the Gaussian output in the upper-left, and the three Binomial outputs in the lower-left, upper-right, and lower-right. Within each square, the left-lower-triangular results are the p-values from each wilcoxon rank sum test, while the right-upper-triangular results are the rank-biserial correlations representing effect sizes.

		GAUSSIAN				BINOMIAL			
		GP.m	brms.f	brms.m	GP.f	GP.m	brms.f	brms.m	GP.f
1	GP.m	-	-0.598	-0.599	-0.447	-	-0.974	-0.776	-0.197
	brms.f	<.001	-	-0.014	0.134	<.001	-	0.989	0.859
	brms.m	<.001	0.423	-	0.135	<.001	<.001	-	0.503
	GP.f	<.001	<.001	<.001	-	<.001	<.001	<.001	-
2	GP.m	-	-0.358	-0.360	-0.356	-	-0.940	-0.680	0.417
	brms.f	<.001	-	-0.088	-0.008	<.001	-	0.881	0.817
	brms.m	<.001	<.001	-	-0.005	<.001	<.001	-	0.643
	GP.f	<.001	1.000	1.000	-	<.001	<.001	<.001	-

Table 3 Results for the RCT data set, comparing between populations of losses for each modelling method, with the Gaussian output in the upper-left, and the three Binomial outputs in the lower-left, upper-right, and lower-right. Within each square, the left-lower-triangular results are the p-values from each wilcoxon rank sum test, while the right-upper-triangular results are the rank-biserial correlations representing effect sizes.

For the continuous outputs, the GP.m model outperforms the three other methods in prediction, while the GP.f model performs slightly better or equally well as the brms models.

Parameter posterior summaries are presented for all four models trained on this data set in tables A9 to A12.

5 | DISCUSSION

In this work, we have demonstrated that the repeated measurements used in applied medical research can be used to scale complex Bayesian nonparametric Gaussian Process models to practical clinical questions. The more complex models have showed to have increased predictive ability compared to the widely-used parametric models, indicating that this may be worthwhile, if achieving optimal model specification is a concern.

Model specification is particularly relevant in medical work when there are specific clinical questions or causal hypotheses to investigate: a poorly-specified model is prone to bias estimates of the parameters of interest and hence possibly give misleading results. The question remains as to how to represent clinical hypotheses within a GP framework: while in principle parametric regression models with finite linear combinations of features have corresponding covariance function representations, it may not be straightforward to interpret covariance function variances and lengthscales in a practical way. Preexisting familiarity with ANOVA and similar models that explain contributions to the variance rather than the functional form of the mean may be a helpful reference point.

For randomised data, in which one of the covariate dimensions has been generated by randomised interventions, it is common to estimate causal effects with parametric models, sometimes including other covariates to increase power. Such estimates will be potentially biased by the limited expressive capabilities of the parametric representation and corresponding model misspecification issues. If including other covariates, the covariance function representation would have the advantage of including more flexible function spaces that might more accurately reflect the true generative process, with interpretation of the parameters associated with non-randomised covariates being less important. We can therefore expect a more accurate estimation of the underlying causal effect when using a more flexible nonparametric model.

With non-randomised observational data, we may still be interested in achieving some insight into the causal mechanism underlying the data, with all of the appropriate caveats of potential confounding. In this case, the covariance function representation may still help by providing a more flexible function space that increases precision of the causal estimate of interest, and possibly reducing the bias of the estimated causal effect by more accurately modelling the influence of observed confounders.

The separability of the covariance functions necessary to exploit Kronecker structure is potentially an important limitation: it is somewhat analogous to being forced to include interaction effects in a parametric model. If the practitioner is interested in extracting a standalone main effect for the purposes of interpretation, or encoding separate mean functions as random effects at an individual level, then this may hinder interpretation. Further work exploring the interpretation of additively structured Kronecker sub-components would help to elucidate the implications of this constraint. As observed earlier, the stricter constraint of having the training data lie on a (mostly) complete grid is obeyed surprisingly frequently in clinical research, as the importance of performing repeated measurements to isolate different contributions to variation is well-understood.

The use of a Gaussian Process object also opens up the possibility of using Bayesian Optimization² type algorithms to measure new data points that are optimally informative, according to some acquisition function. The analytical posterior mean and variance of the latent GP object could be used to assess which unsampled areas of the covariate space would be best explored to reduce uncertainty in the effect of interest. Given the relatively strict grid structure necessary, performing this iteratively may be challenging, but the posterior predictive estimates provided by the fitted GPs could still be used to motivate future research study designs.

In conclusion, in this article, we have demonstrated the ability and utility of scaling Gaussian Process models to large real-world clinical data sets through the use of Kronecker-structure covariance matrices and repeated measurements in the data.

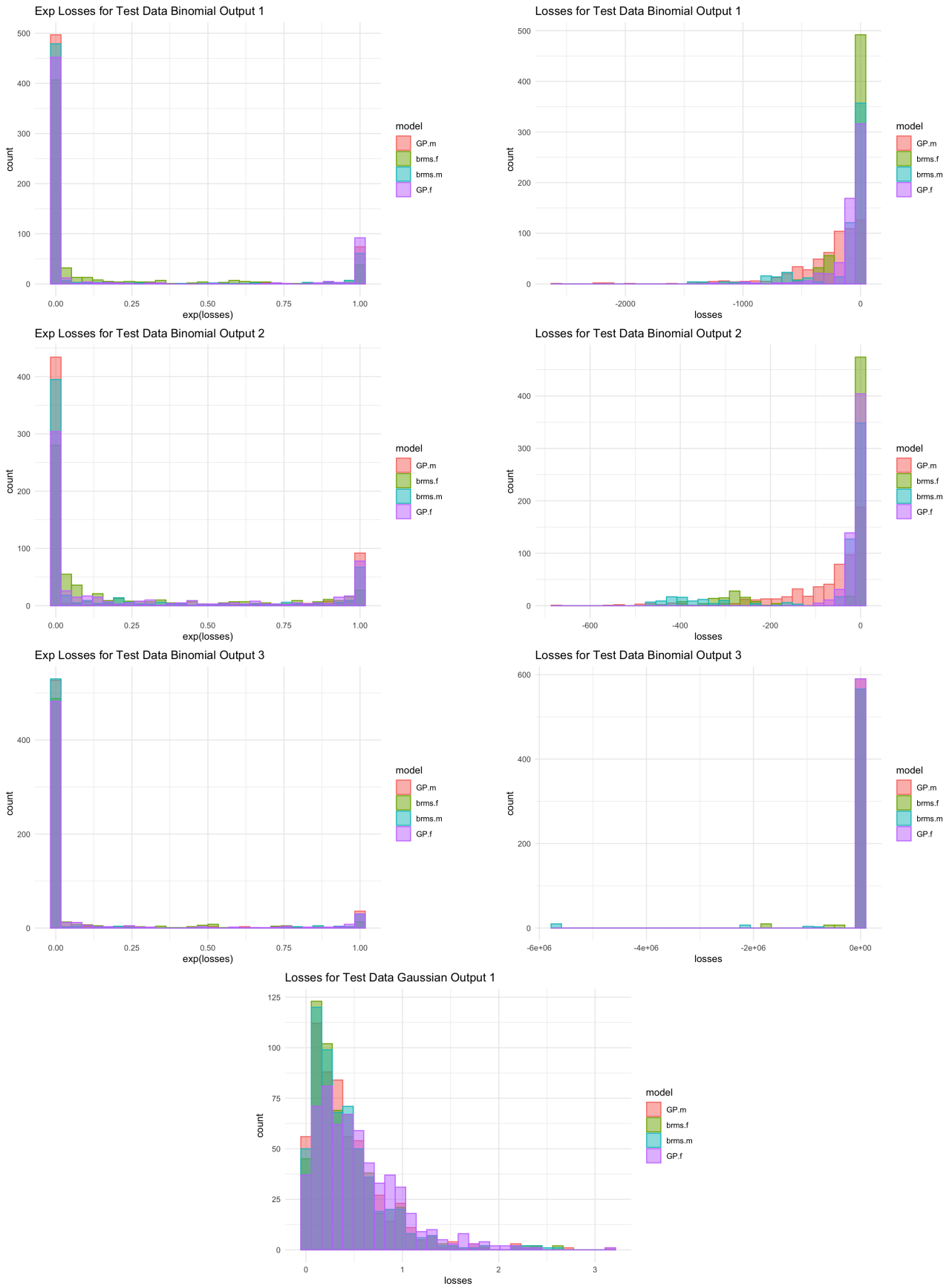


Figure 4 Figures for the observational time series data set, representing histograms of losses for each of the method for each of the outputs. Binomial outputs are plotted in the first three rows, with those on the left on the exponentiated probability scale, and those on the right the same results plotted on the original logarithmic scale. The lowest-left plot represents the losses on the one continuous output

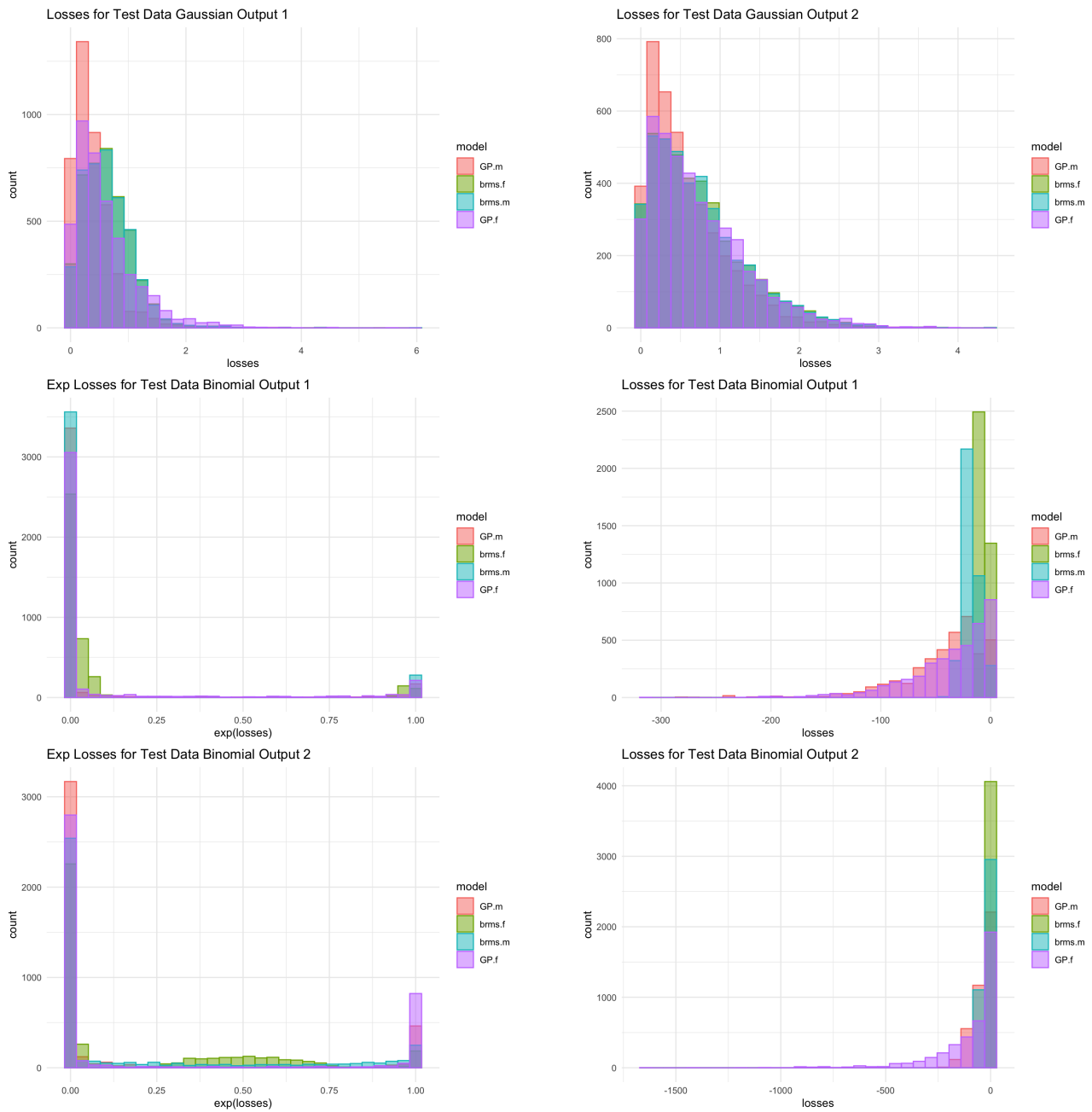


Figure 5 Figures for the RCT data example, representing histograms of losses for each of the method for each of the outputs. Binomial outputs are plotted in the first two rows, with those on the left on the exponentiated probability scale, and those on the right the same results plotted on the original logarithmic scale. The lowest two plots represent the losses on the two Gaussian-distributed outputs.

ACKNOWLEDGMENTS

We thank Thien Trung Tran, Cathrine Helgestad Kristiansen and Peter Lauritzen for providing the radiological data used in this article.

Author contributions

OT helped with conceptualising the project, constructing the code, running the experiments, and writing the manuscript. LR helped with model design, providing the starting codebase, writing the manuscript, and deriving theoretical results.

Financial disclosure

None reported.

Conflict of interest

The authors declare no potential conflict of interests.

How to cite this article: Thomas O., L. Rønneberg (2024), Heterogeneous Clinical Trial Outcomes via Multi-Output Gaussian Processes, *arxiv.org*, 2024;00:1–6.

APPENDIX

A STAN OUTPUTS

	mean	sd	l-95% CI	u-95% CI	n.eff	Rhat
ρ_1	1.404	0.173	1.087	1.771	321.774	1.006
ρ_2	0.97	0.076	0.823	1.12	947.797	1.007
ρ_3	1.193	0.112	0.959	1.408	202.334	1.009
α_1	0.982	0.143	0.752	1.31	623.841	1.003
α_2	1.497	0.273	1.048	2.113	304.171	1.007
α_3	1.005	0.279	0.575	1.652	1373.194	1.005
α_4	1.735	0.42	1.068	2.718	609.914	1.006
$\alpha_1^{(n)}$	0.106	0.007	0.093	0.119	1916.695	1.002
$\alpha_2^{(n)}$	0.132	0.009	0.115	0.149	650.408	1.001
$L_{21}^{(n)}$	-0.005	0.09	-0.185	0.169	2174.739	1.001
$L_{22}^{(n)}$	0.996	0.006	0.98	1	2543.158	1
L_{21}	-0.135	0.143	-0.416	0.149	439.501	1.006
L_{22}	0.98	0.025	0.909	1	476.384	1.007
L_{31}	0.686	0.143	0.365	0.903	2331.114	1
L_{32}	-0.08	0.196	-0.432	0.319	2916.251	1
L_{33}	0.667	0.137	0.393	0.912	1995.937	1.001
L_{41}	-0.034	0.163	-0.347	0.278	644.503	1.003
L_{42}	0.867	0.085	0.646	0.976	2074.728	1
L_{43}	-0.022	0.184	-0.392	0.336	1443.446	1.002
L_{44}	0.4	0.137	0.165	0.701	1730.865	1

Table A1 Posterior summaries of the interpretable parameters of the GP.f model from the first CV fold on the simulated data example from Section 4.4

	mean	sd	l-95% CI	u-95% CI	n.eff	Rhat
ρ_1	1.833	0.171	1.507	2.188	630.434	1.004
ρ_2	1.018	0.064	0.897	1.146	1156.583	1.004
ρ_3	24.54	32.778	5.98	89.383	1883.495	1.003
α_1	0.746	0.095	0.579	0.954	889.352	1.003
α_2	2.076	0.261	1.613	2.624	577.406	1.007
α_3	0.863	0.264	0.48	1.487	1686.661	1.002
α_4	2.464	0.541	1.541	3.632	1534.739	1.003
$\alpha_1^{(n)}$	0.104	0.007	0.092	0.118	2983.666	1.001
$\alpha_2^{(n)}$	0.101	0.007	0.088	0.115	1881.657	1.001
$L_{21}^{(n)}$	-0.207	0.09	-0.383	-0.025	3693.566	1
$L_{22}^{(n)}$	0.974	0.02	0.924	0.999	3455.251	0.999
L_{21}	-0.183	0.126	-0.416	0.076	364.228	1.01
L_{22}	0.975	0.025	0.91	1	411.066	1.008
L_{31}	0.605	0.164	0.226	0.865	2594.035	1.002
L_{32}	-0.046	0.221	-0.46	0.398	3936.939	1
L_{33}	0.734	0.132	0.456	0.955	2001.942	1.003
L_{41}	-0.144	0.141	-0.405	0.147	599.615	1.006
L_{42}	0.85	0.08	0.664	0.964	2309.363	1
L_{43}	-0.039	0.19	-0.424	0.324	1337.541	1.008
L_{44}	0.421	0.127	0.184	0.675	2178.473	1
σ_{re}^2	0.058	0.012	0.039	0.086	1102.067	1.004

Table A2 Posterior summaries of the interpretable parameters of the GP.m model from the first CV fold on the simulated data example from Section 4.4

	Estimate	sd	l-95% CI	u-95% CI	Rhat	Bulk.ESS	Tail.ESS
y1.Intercept	0.002	0.068	-0.134	0.135	1.001	5464.966	3092.083
y2.Intercept	-0.161	0.055	-0.268	-0.055	1.002	4786.035	2940.475
y3.Intercept	0.058	0.147	-0.234	0.345	1	5457.726	3301.1
y4.Intercept	-0.265	0.173	-0.611	0.068	1	5162.581	2977.072
y1.x1	0.234	0.082	0.075	0.396	1.002	5932.14	3073.043
y1.x2	0.421	0.073	0.277	0.565	1	5867.37	2870.77
y1.x3	-0.03	0.078	-0.185	0.121	1	4867.733	2544.01
y2.x1	-0.49	0.067	-0.623	-0.362	1	4672.154	2914.568
y2.x2	0.446	0.059	0.335	0.559	1	4995.344	2801.483
y2.x3	0.359	0.062	0.24	0.477	1.001	4879.298	3101.912
y3.x1	0.043	0.182	-0.304	0.388	1.002	5430.894	3058.107
y3.x2	0.078	0.16	-0.23	0.386	1.001	6038.251	3178.676
y3.x3	-0.032	0.169	-0.36	0.301	1.001	5622.199	3016.555
y4.x1	-0.913	0.217	-1.349	-0.507	1	5067.848	3007.645
y4.x2	0.933	0.209	0.538	1.356	1.003	4827.501	3173.996
y4.x3	0.435	0.193	0.06	0.809	1	4120.251	3021.145

Table A3 Posterior summaries of the parameters of the brms.f model from the first CV fold on the simulated data example from Section 4.4

	Estimate	sd	l-95% CI	u-95% CI	Rhat	Bulk.ESS	Tail.ESS
y1.Intercept	0.002	0.077	-0.151	0.152	1.001	6402.526	2842.214
y2.Intercept	-0.15	0.286	-0.736	0.438	1.001	1398.978	1713.599
y3.Intercept	0.06	0.183	-0.297	0.418	1.001	4684.172	2849.119
y4.Intercept	-0.288	0.546	-1.362	0.854	1.001	1799.947	2199.357
y1.x1	0.235	0.082	0.07	0.391	1	9351.66	2680.745
y1.x2	0.423	0.073	0.28	0.565	1.002	9552.251	3006.171
y1.x3	-0.028	0.09	-0.197	0.151	1.001	5891.755	3109.685
y2.x1	-0.49	0.029	-0.546	-0.434	1	8431.978	2622.935
y2.x2	0.445	0.025	0.397	0.492	1.001	8605.844	2679.603
y2.x3	0.35	0.324	-0.333	0.996	1.002	1828.779	2024.193
y3.x1	0.046	0.183	-0.315	0.399	1.001	7798.346	3147.908
y3.x2	0.078	0.155	-0.23	0.387	1.003	8106.717	2825.376
y3.x3	-0.03	0.219	-0.451	0.391	1	4265.744	2471.228
y4.x1	-1.154	0.257	-1.671	-0.668	1.001	6917.828	2769.571
y4.x2	1.182	0.257	0.712	1.701	1.003	8080.056	3051.224
y4.x3	0.577	0.614	-0.656	1.874	1.001	2099.679	2356.275

Table A4 Posterior summaries of the parameters of the brms.m model from the first CV fold on the simulated data example from Section 4.4

	mean	sd	l-95% CI	u-95% CI	n.eff	Rhat
Side	0.138	0.037	0.08	0.226	1514.041	1.002
Time	0.282	0.021	0.244	0.326	479.861	1.003
TubeVoltage	0.298	0.099	0.151	0.539	3460.95	1
Sex	1.057	0.218	0.689	1.545	2129.349	1.004
Age	0.32	0.092	0.217	0.602	75.444	1.026
KbyV	0.976	0.253	0.338	1.391	97.965	1.017
α_1	0.584	0.049	0.495	0.686	946.77	1.007
α_2	6.708	2.442	3.748	12.746	902.727	1.008
α_3	2.963	0.593	2.029	4.351	1385.233	1.006
α_4	5.118	3.198	2.613	11.731	233.638	1.017
$\alpha_1^{(n)}$	0.447	0.017	0.415	0.481	1109.652	1.002
L_{21}	0.767	0.072	0.607	0.884	705.094	1.002
L_{22}	0.632	0.085	0.468	0.795	684.22	1.002
L_{31}	0.813	0.06	0.677	0.91	1004.867	1.001
L_{32}	0.512	0.091	0.338	0.691	974.675	1.001
L_{33}	0.249	0.053	0.154	0.361	1884.588	0.999
L_{41}	0.776	0.076	0.604	0.903	700.609	1.004
L_{42}	0.486	0.114	0.26	0.695	693.147	1.004
L_{43}	-0.205	0.096	-0.386	-0.011	1136.005	1
L_{44}	0.292	0.079	0.146	0.45	1506.603	1

Table A5 Posterior summaries of the interpretable parameters of the GP.f model from the first CV fold on the observational time series example from Section 4.5

	mean	sd	l-95% CI	u-95% CI	n.eff	Rhat
Side	0.811	0.171	0.527	1.205	1923.84	1.001
Time	0.257	0.017	0.225	0.292	507.519	1.005
TubeVoltage	0.249	0.097	0.117	0.48	3308.898	1
Sex	1.147	0.286	0.699	1.791	3691.531	1
Age	17.824	38.394	5.412	59.024	1914.216	1.002
KbyV	6.986	3.715	3.664	14.81	1589.906	1
α_1	0.424	0.052	0.335	0.536	1307.983	1.004
α_2	9.917	6.899	3.258	29.889	1739.195	1.002
α_3	6.743	4.765	2.485	20.149	973.293	1.001
α_4	6.568	5.372	1.985	22.38	1717.292	1.002
$\alpha_1^{(n)}$	0.334	0.016	0.303	0.366	582.19	1.003
L_{21}	0.242	0.089	0.064	0.415	2003.83	1.002
L_{22}	0.966	0.023	0.91	0.998	2010.449	1.001
L_{31}	0.354	0.085	0.18	0.511	1985.88	1
L_{32}	0.848	0.045	0.748	0.926	1860.018	1.002
L_{33}	0.377	0.065	0.256	0.514	1790.967	1.004
L_{41}	0.211	0.099	0.016	0.402	2336.426	1
L_{42}	0.785	0.065	0.639	0.891	2637.555	1.001
L_{43}	-0.33	0.121	-0.551	-0.078	1495.683	1.002
L_{44}	0.438	0.107	0.226	0.64	1183.002	1.002
σ_{re}^2	0.907	0.227	0.537	1.403	1096.364	1.001

Table A6 Posterior summaries of the interpretable parameters of the GP.m model from the first CV fold on the observational time series example from Section 4.5

	Estimate	sd	l-95% CI	u-95% CI	Rhat	Bulk.ESS	Tail.ESS
HU.Intercept	-1.39	0.074	-1.537	-1.247	1	2409.083	2984.331
Peter.Intercept	-23.136	15.093	-62.433	-6.119	1.003	608.858	576.982
Sumit.Intercept	-23.363	18.786	-77.043	-5.53	1.006	409.13	320.44
Thien.Intercept	-29.083	19.913	-70.655	-7.379	1.003	691.947	498.643
HU.Sex	-0.254	0.051	-0.357	-0.154	1.001	4559.867	2846.231
HU.Age	-0.082	0.022	-0.125	-0.039	1.001	4361.788	2682.417
HU.KbyV	0.15	0.028	0.094	0.207	1.001	3720.045	3164.562
HU.TubeVoltage	-0.007	0.061	-0.125	0.114	1	3883.938	3248.508
HU.Side	-0.034	0.043	-0.12	0.05	1	4765.954	2693.787
HU.Times.1	0.772	0.08	0.615	0.926	1.001	2144.028	2807.039
HU.Times.2	1.699	0.082	1.537	1.866	1.001	2219.165	2908.287
HU.Times.3	2.093	0.083	1.932	2.262	1	2269.678	2760.094
HU.Times.4	2.161	0.08	2.003	2.318	1.001	2205.402	2842.623
HU.Times.5	2.16	0.081	1.998	2.32	1.001	2183.258	2429.128
HU.Times.6	2.159	0.081	2.003	2.317	1	2267.362	3046.82
Peter.Sex	-1.596	0.392	-2.383	-0.842	1.001	3919.9	3341.905
Peter.Age	-0.625	0.151	-0.931	-0.34	1.002	5417.444	2985.744
Peter.KbyV	0.296	0.19	-0.07	0.679	1	3325.893	2899.162
Peter.TubeVoltage	1.505	0.421	0.662	2.33	1.002	2808.877	2631.265
Peter.Side	0.101	0.283	-0.439	0.659	1	5410.548	2982.479
Peter.Times.1	19.842	15.096	2.695	58.589	1.003	609.021	557.101
Peter.Times.2	23.304	15.094	6.205	62.54	1.003	608.571	545.979
Peter.Times.3	25.541	15.108	8.451	64.9	1.003	607.598	567.206
Peter.Times.4	25.885	15.102	8.738	65.16	1.002	613.898	549.396
Peter.Times.5	26.028	15.118	8.906	65.348	1.003	611.03	581.704
Peter.Times.6	26.01	15.096	8.902	65.252	1.003	612.908	577.387
Sumit.Sex	-1.364	0.325	-2.022	-0.746	1	4423.775	2895.507
Sumit.Age	-0.551	0.127	-0.793	-0.303	1.001	5916.021	2742.276
Sumit.KbyV	0.5	0.154	0.205	0.808	1.001	3755.939	2738.673
Sumit.TubeVoltage	1.049	0.349	0.38	1.754	1.001	3319.896	2957.351
Sumit.Side	-0.034	0.231	-0.495	0.415	1	5586.167	2965.208
Sumit.Times.1	20.573	18.783	2.707	74.057	1.006	408.385	317.588
Sumit.Times.2	23.32	18.79	5.438	76.846	1.006	408.887	320.442
Sumit.Times.3	25.238	18.792	7.402	79.115	1.006	409.265	319.583
Sumit.Times.4	25.295	18.788	7.376	78.9	1.005	409.093	321.446
Sumit.Times.5	25.529	18.783	7.659	78.986	1.005	409.948	320.44
Sumit.Times.6	24.87	18.781	7.055	78.473	1.006	409.119	321.843
Thien.Sex	-1.093	0.516	-2.116	-0.103	1.001	3390.629	2920.511
Thien.Age	-0.562	0.208	-0.988	-0.157	1	5525.843	2864.83
Thien.KbyV	-0.035	0.276	-0.577	0.509	1	3796.754	3311.912
Thien.TubeVoltage	2.026	0.607	0.854	3.222	1	3172.331	2965.172
Thien.Side	0.195	0.405	-0.585	0.973	1.001	5236.692	2325.445
Thien.Times.1	24.506	19.934	2.887	66.063	1.003	691.319	479.517
Thien.Times.2	28.927	19.911	7.254	70.355	1.003	692.155	495.169
Thien.Times.3	32.396	19.948	10.587	74.065	1.003	689.624	489.518
Thien.Times.4	34.038	19.995	11.864	75.923	1.003	691.37	485.938
Thien.Times.5	34.031	19.989	11.909	76.187	1.003	695.89	504.097
Thien.Times.6	33.999	19.993	11.874	76.105	1.003	683.468	502.573

Table A7 Posterior summaries of the parameters of the brms.f model from the first CV fold on the observational time series example from Section 4.5

	Estimate	sd	l-95% CI	u-95% CI	Rhat	Bulk.ESS	Tail.ESS
HU.Intercept	-1.387	0.105	-1.591	-1.18	1.001	1618.397	2350.325
Peter.Intercept	-33.07	17.474	-76.833	-11.798	1.001	610.753	403.092
Sumit.Intercept	-29.19	28.557	-141.511	-8.163	1.033	96.551	22.218
Thien.Intercept	-47.712	25.873	-119.681	-16.076	1.005	397.244	235.653
HU.Sex	-0.249	0.104	-0.457	-0.045	1	1274.419	1887.114
HU.Age	-0.083	0.045	-0.171	0.006	1.001	1298.837	1541.561
HU.KbyV	0.152	0.055	0.042	0.258	1.003	1179.928	2072.619
HU.TubeVoltage	-0.003	0.12	-0.239	0.235	1.001	1153.473	1620.713
HU.Side	-0.03	0.038	-0.104	0.044	1.007	8636.042	2727.371
HU.Times.1	0.772	0.069	0.636	0.906	1.001	3222.682	3355.595
HU.Times.2	1.701	0.071	1.563	1.837	1	3227.142	3142.511
HU.Times.3	2.092	0.072	1.95	2.233	1	3132.795	3264.571
HU.Times.4	2.16	0.07	2.019	2.301	1.001	3122.661	2327.567
HU.Times.5	2.16	0.07	2.024	2.303	1.001	3183.713	3003.711
HU.Times.6	2.15	0.072	2.007	2.29	1.001	3253.032	3026.83
Peter.Sex	-4.558	1.801	-8.348	-1.288	1.001	1423.471	2296.226
Peter.Age	-1.553	0.759	-3.166	-0.149	1	1302.35	2167.791
Peter.KbyV	0.033	0.909	-1.802	1.771	1.004	1102.953	1896.869
Peter.TubeVoltage	3.637	1.948	-0.117	7.662	1.001	1250.605	1622.67
Peter.Side	0.315	0.414	-0.483	1.116	1.001	8134.444	3079.231
Peter.Times.1	25.238	17.369	4.68	68.967	1.002	610.631	399.844
Peter.Times.2	34.946	17.552	13.457	79.709	1.001	603.05	408.878
Peter.Times.3	40.177	17.659	18.292	85.207	1.001	598.898	406.589
Peter.Times.4	40.714	17.667	18.804	85.767	1.001	600.787	407.753
Peter.Times.5	40.987	17.666	19.086	85.603	1.001	604.068	428.653
Peter.Times.6	40.957	17.673	19.018	85.762	1.001	612.928	424.599
Sumit.Sex	-2.38	1.079	-4.695	-0.294	1.001	1356.179	1981.976
Sumit.Age	-0.942	0.444	-1.834	-0.11	1.003	1391.182	2059.489
Sumit.KbyV	0.857	0.56	-0.212	1.956	1.003	1385.784	2115.462
Sumit.TubeVoltage	1.7	1.175	-0.576	4.029	1.002	1272.342	1796.238
Sumit.Side	-0.081	0.301	-0.675	0.496	1.001	7380.028	2808.069
Sumit.Times.1	24.668	28.559	3.78	137.087	1.031	104.278	22.229
Sumit.Times.2	29.354	28.572	8.362	141.328	1.031	103.682	22.201
Sumit.Times.3	32.853	28.572	11.76	144.49	1.032	103.688	22.119
Sumit.Times.4	32.896	28.569	11.864	144.481	1.031	103.616	22.181
Sumit.Times.5	33.322	28.568	12.247	144.342	1.032	103.926	22.156
Sumit.Times.6	32.2	28.571	11.09	144.183	1.032	103.205	22.143
Thien.Sex	-2.909	2.095	-7.371	0.794	1.001	1832.914	2101.764
Thien.Age	-1.337	0.879	-3.253	0.247	1.001	1666.775	2237.486
Thien.KbyV	-0.32	1.08	-2.498	1.775	1.004	1420.407	2315.322
Thien.TubeVoltage	5.034	2.561	0.484	10.854	1	1559.872	1907.257
Thien.Side	0.637	0.608	-0.522	1.839	1.003	6508.089	2826.776
Thien.Times.1	36.157	25.34	5.81	108.251	1.004	402.642	236.309
Thien.Times.2	48.473	25.996	16.357	121.175	1.004	391.273	239.821
Thien.Times.3	55.615	26.395	22.403	128.826	1.004	389.505	234.506
Thien.Times.4	57.812	26.517	24.452	130.267	1.005	390.179	235.505
Thien.Times.5	57.797	26.51	24.464	130.758	1.004	393.287	238.189
Thien.Times.6	57.725	26.516	24.307	131.551	1.004	391.34	230.294

Table A8 Posterior summaries of the parameters of the brms.m model from the first CV fold on the observational time series example from Section 4.5

	mean	sd	l-95% CI	u-95% CI	n.eff	Rhat
Location.Iliac	1.286	0.074	1.146	1.439	1513.542	1.003
Location.Femoral	9.77	1.739	7.113	14.038	445.735	1.005
Location.Popliteal	14.298	4.277	8.887	23.962	561.439	1.003
keV.40	0.237	0.026	0.187	0.29	759.765	1.002
keV.50	0.113	0.014	0.088	0.142	744.719	1.002
Randomisation	0.292	0.038	0.228	0.37	633.115	1.009
Sex	1.052	0.078	0.905	1.212	1591.639	1.007
Age	0.237	0.015	0.202	0.265	44.326	1.092
Flow	0.348	0.03	0.305	0.439	38.1	1.116
α_1	1.012	0.054	0.914	1.128	480.564	1.003
α_2	0.619	0.035	0.555	0.691	758.82	1.001
α_3	4.936	0.776	3.694	6.722	1065.099	1.002
α_4	15.009	2.419	11.154	20.61	1338.5	1
$\alpha_1^{(n)}$	0.294	0.004	0.286	0.303	1306.745	1.003
$\alpha_2^{(n)}$	0.715	0.009	0.697	0.733	1576.561	1.001
$L_{21}^{(n)}$	-0.144	0.019	-0.181	-0.107	2935.456	1.001
$L_{22}^{(n)}$	0.989	0.003	0.984	0.994	2885.614	1.001
L_{21}	0.732	0.033	0.661	0.79	694.7	1.003
L_{22}	0.68	0.035	0.613	0.75	700.848	1.003
L_{31}	0.602	0.044	0.512	0.685	1118.582	1.003
L_{32}	-0.032	0.073	-0.176	0.114	905.705	1.007
L_{33}	0.793	0.034	0.722	0.857	1132.266	1.002
L_{41}	0.71	0.031	0.647	0.767	985.695	1.003
L_{42}	-0.015	0.061	-0.135	0.104	492.138	1.006
L_{43}	0.321	0.057	0.205	0.429	511.796	1.012
L_{44}	0.619	0.038	0.545	0.693	628.993	1.005

Table A9 Posterior summaries of the interpretable parameters of the GP.f model from the first CV fold on the RCT example from Section 4.6

	mean	sd	l-95% CI	u-95% CI	n.eff	Rhat
Location.Iliac	1.071	0.095	0.9	1.275	496.725	1.008
Location.Femoral	1.69	0.112	1.482	1.931	718.188	1.002
Location.Popliteal	1.776	0.125	1.552	2.039	640.221	1.005
keV.40	0.102	0.012	0.079	0.127	1185.38	1.002
keV.50	0.054	0.007	0.041	0.068	1123.026	1
Randomisation	0.12	0.026	0.078	0.18	1160.001	1
Sex	1.31	0.166	1.022	1.668	2934.555	1
Age	35.694	12.951	19.5	69.44	812.477	1.004
Flow	11.488	2.314	7.528	16.652	471.008	1.001
α_1	1	0.077	0.861	1.16	691.075	1.006
α_2	1.317	0.113	1.11	1.548	632.407	1.006
α_3	8.796	1.699	6.114	12.616	909.123	1.005
α_4	14.696	3.03	10.203	21.863	877.625	1.005
$\alpha_1^{(n)}$	0.243	0.003	0.237	0.249	2819.81	1
$\alpha_2^{(n)}$	0.567	0.008	0.552	0.582	1474.628	1
$L_{21}^{(n)}$	-0.12	0.018	-0.158	-0.085	2945.145	1
$L_{22}^{(n)}$	0.993	0.002	0.988	0.996	2900.402	1
L_{21}	0.295	0.041	0.217	0.374	770.558	1.004
L_{22}	0.955	0.013	0.927	0.976	768.216	1.004
L_{31}	0.46	0.046	0.366	0.546	1245.77	1.002
L_{32}	-0.282	0.071	-0.416	-0.137	1191.492	1.003
L_{33}	0.837	0.033	0.771	0.898	1171.472	1.003
L_{41}	0.377	0.042	0.292	0.458	978.818	1.001
L_{42}	-0.053	0.061	-0.169	0.067	932.93	1.005
L_{43}	0.106	0.079	-0.046	0.262	277.257	1.011
L_{44}	0.912	0.02	0.871	0.948	907.221	1.003
σ_{re}^2	0.121	0.018	0.09	0.159	769.687	1.003

Table A10 Posterior summaries of the interpretable parameters of the GP.m model from the first CV fold on the RCT example from Section 4.6

	Estimate	sd	l-95% CI	u-95% CI	Rhat	Bulk.ESS	Tail.ESS
HU.Intercept	0.275	0.04	0.196	0.357	1	10453.102	2692.506
SD.Intercept	-0.368	0.048	-0.462	-0.273	1.002	8602.66	3274.616
Sumit.Intercept	2.844	0.224	2.408	3.296	1.001	7851.73	3100.73
DanLevi.Intercept	2.046	0.158	1.735	2.343	1	7434.289	2993.31
HU.Sex	-0.043	0.029	-0.1	0.014	0.999	7290.619	3315.779
HU.Age	0.076	0.013	0.051	0.101	1.001	8695.496	2708.414
HU.Flowmls	0.149	0.015	0.119	0.178	1	7565.725	3049.803
HU.Side	0	0.027	-0.05	0.054	1.001	8424.888	3120.189
HU.Location	-0.085	0.013	-0.11	-0.059	1.001	9835.406	2940.605
HU.keV	-0.625	0.013	-0.65	-0.6	1.005	9179.524	2829.488
SD.Sex	-0.272	0.034	-0.339	-0.204	1.001	7248.65	3262.452
SD.Age	-0.021	0.015	-0.051	0.009	1	8169.73	3188.157
SD.Flowmls	0.226	0.018	0.192	0.261	1.003	7449.155	3557.409
SD.Side	0.091	0.032	0.028	0.156	1.001	8420.121	3258.472
SD.Location	0.183	0.015	0.153	0.213	1.001	9028.951	2844.361
SD.keV	-0.271	0.015	-0.301	-0.241	1.001	10044.46	2975.49
Sumit.Sex	0.053	0.16	-0.268	0.357	1	7327.927	3328.309
Sumit.Age	-0.088	0.073	-0.234	0.049	1	10120.038	3351.897
Sumit.Flowmls	0.067	0.081	-0.093	0.22	1	6514.66	3419.375
Sumit.Side	0.139	0.148	-0.152	0.432	1.002	8806.937	2611.821
Sumit.Location	0.006	0.068	-0.127	0.141	1.002	8812.139	2832.606
Sumit.keV	-0.847	0.069	-0.988	-0.717	1.001	6880.567	3395.213
DanLevi.Sex	0.204	0.115	-0.024	0.43	1.001	7937.028	2831.09
DanLevi.Age	0.02	0.05	-0.078	0.115	1.002	9383.669	2899.218
DanLevi.Flowmls	0.194	0.057	0.083	0.308	1	7261.622	3446.642
DanLevi.Side	0.042	0.101	-0.153	0.244	1	8716.294	3142.675
DanLevi.Location	-0.141	0.047	-0.231	-0.05	1.002	7775.343	2986.236
DanLevi.keV	-1.296	0.05	-1.396	-1.197	1	6444.788	3221.858

Table A11 Posterior summaries of the parameters of the brms.f model from the first CV fold on the RCT example from Section 4.6

	Estimate	sd	l-95% CI	u-95% CI	Rhat	Bulk.ESS	Tail.ESS
HU.Intercept	0.238	0.088	0.062	0.401	1.026	187.541	469.566
SD.Intercept	-0.386	0.075	-0.535	-0.24	1.005	418.06	1129.855
Sumit.Intercept	5.513	0.645	4.332	6.825	1.006	724.949	1647.996
DanLevi.Intercept	5.439	0.802	3.937	7.059	1.009	402.24	958.231
HU.Sex	-0.024	0.121	-0.247	0.218	1.028	173.245	268.353
HU.Age	0.078	0.049	-0.017	0.174	1.019	255.92	531.007
HU.Flowmls	0.152	0.059	0.039	0.267	1.016	210.331	380.7
HU.Side	0.004	0.014	-0.024	0.032	1	5957.802	2980.97
HU.Location	-0.075	0.007	-0.088	-0.062	1.002	6749.447	2902.081
HU.keV	-0.626	0.007	-0.639	-0.612	1.001	8216.338	2970.541
SD.Sex	-0.268	0.092	-0.438	-0.084	1.009	305.963	568.382
SD.Age	-0.024	0.037	-0.097	0.048	1.011	408.812	947.47
SD.Flowmls	0.222	0.044	0.135	0.308	1.006	347.06	930.257
SD.Side	0.089	0.029	0.032	0.145	1.002	5594.598	2939.804
SD.Location	0.19	0.013	0.164	0.216	1.001	6120.002	3129.237
SD.keV	-0.272	0.013	-0.297	-0.246	1.001	6320.706	2932.901
Sumit.Sex	0.267	0.698	-1.066	1.655	1.008	347.219	766.086
Sumit.Age	-0.128	0.313	-0.771	0.46	1.012	502.922	1384.839
Sumit.Flowmls	-0.034	0.356	-0.761	0.64	1.004	405.3	786.352
Sumit.Side	0.25	0.193	-0.132	0.636	1.002	4853.972	2810.804
Sumit.Location	0.006	0.085	-0.158	0.172	1.001	5430.007	3161.704
Sumit.keV	-1.257	0.095	-1.451	-1.077	1.001	5131.408	3045.637
DanLevi.Sex	0.803	0.974	-1.141	2.675	1.008	305.69	595.933
DanLevi.Age	-0.169	0.426	-1.004	0.67	1.007	462.015	1039.884
DanLevi.Flowmls	0.285	0.496	-0.7	1.238	1.002	410.709	1011.654
DanLevi.Side	0.14	0.19	-0.231	0.503	1	5126.812	3077.509
DanLevi.Location	-0.39	0.091	-0.565	-0.21	1	4979.411	3335.896
DanLevi.keV	-3.116	0.136	-3.389	-2.86	1	3505.023	2501.601

Table A12 Posterior summaries of the parameters of the brms.m model from the first CV fold on the RCT example from Section 4.6

B RANDOM EFFECTS IN THE INTRINSIC COREGIONALIZATION MODEL

In this appendix, we demonstrate the effect of adding a random effect to an Intrinsic Coregionalization Model (ICM), in the simplest case where the covariance functions over the inputs and the outputs are both linear. Recall that the ICM for a multi-output GP over m outputs can be written as

$$\begin{bmatrix} f_1 \\ \vdots \\ f_m \end{bmatrix} \sim \mathcal{GP}(0, \mathbf{B} \kappa_x(x, x')), \quad (\text{B1})$$

where \mathbf{B} is the $m \times m$ coregionalisation matrix giving the covariance over the outputs, and $\kappa_x(x, x')$ the covariance function over the inputs. In the case of a fully observed dataset, we can write this using the Kronecker product $\mathbf{f}(\mathbf{X}) \sim \mathcal{N}(0, \mathbf{B} \otimes \mathbf{K}_x)$. By exploiting the connections between Gaussian Processes and Bayesian linear regression, in the case of a linear kernel over the inputs, $\kappa_x(\mathbf{x}, \mathbf{x}') = 1 + \mathbf{x}^T \mathbf{x}'$, the ICM is equivalent to the following linear model:

$$\begin{bmatrix} \mathbf{f}_1(\mathbf{X}) \\ \vdots \\ \mathbf{f}_m(\mathbf{X}) \end{bmatrix} = \begin{bmatrix} \mathbf{X} & 0 & \cdots & 0 \\ 0 & \mathbf{X} & \cdots & 0 \\ \vdots & \vdots & \ddots & \vdots \\ 0 & 0 & \cdots & \mathbf{X} \end{bmatrix} \begin{bmatrix} \beta_1 \\ \beta_2 \\ \vdots \\ \beta_m \end{bmatrix}, \quad \begin{bmatrix} \beta_1 \\ \beta_2 \\ \vdots \\ \beta_m \end{bmatrix} \sim \mathcal{N}(0, \mathbf{B} \otimes \mathbf{I}_{(p+1)}), \quad (\text{B2})$$

where $\mathbf{X} \in \mathbb{R}^{m \times (p+1)}$ denotes the design matrix of a linear regression including the intercept, $\beta_j \in \mathbb{R}^{(p+1)}$ the corresponding output-specific coefficient vector, and \mathbf{I}_p the p -dimensional identity matrix. Hence, this is equivalent to fitting a linear model to each output, with output-specific coefficients β_j for $j = 1, \dots, m$. Due to the joint distribution over the coefficient vectors, these linear models are correlated in the prior, allowing the models to influence each other, borrowing strength across outputs.

When working with multiple covariance functions, that are multiplied together, we need to consider the effect on the induced feature space. Consider a set of covariates that can be blocked into two sets $\mathbf{X} = [\mathbf{X}^{(1)}, \mathbf{X}^{(2)}]$, where $\mathbf{X}^{(2)}$ correspond to patient-specific covariates, while $\mathbf{X}^{(1)}$ are other covariates in the model. In this paper, we consider covariance structures that decompose across these groups of covariates, e.g. $\kappa(\mathbf{X}, \mathbf{X}') = \kappa_1(\mathbf{X}^{(1)}, \mathbf{X}^{(1)}) \kappa_2(\mathbf{X}^{(2)}, \mathbf{X}^{(2)})$. Generally, multiplying together kernels has the effect of modelling interactions between the covariates, e.g. if both κ_1 and κ_2 are linear kernels, the induced features space is $\phi_{1 \times 2} = \{1, x_1^{(1)}, \dots, x_{p_1}^{(1)}, x_1^{(2)}, \dots, x_{p_2}^{(2)}, x_1^{(1)} x_1^{(2)}, \dots, x_{p_1}^{(1)} x_{p_2}^{(2)}\}$, and GP regression is equivalent to performing a linear regression using the extended basis $\phi_{1 \times 2}$. Similarly in the multi-output setting GP regression becomes equivalent to the model in equation (B2), but with the $m \times ((p_1 + 1)(p_2 + 1))$ matrix $\Phi_{1 \times 2}$ taking the place of X , and modulo some dimensionality changes on the identity matrix in the prior over the coefficients.

Further complicating the model by adding a random effect to κ_2 as in Section 2.5:

$$\begin{bmatrix} f_1 \\ \vdots \\ f_m \end{bmatrix} \sim \mathcal{GP}(0, \mathbf{B} \kappa_1(\mathbf{X}^{(1)}, \mathbf{X}^{(1)}) (\kappa_2(\mathbf{X}^{(2)}, \mathbf{X}^{(2)}) + \gamma^2 \mathbf{I}_m)), \quad (\text{B3})$$

has the effect of adding extra variance to the coefficients corresponding to the non-patient specific covariates. The model becomes

$$\begin{bmatrix} \mathbf{f}_1(\mathbf{X}) \\ \vdots \\ \mathbf{f}_m(\mathbf{X}) \end{bmatrix} = \begin{bmatrix} \Phi_{1 \times 2} & 0 & \cdots & 0 \\ 0 & \Phi_{1 \times 2} & \cdots & 0 \\ \vdots & \vdots & \ddots & \vdots \\ 0 & 0 & \cdots & \Phi_{1 \times 2} \end{bmatrix} \begin{bmatrix} \beta_1 \\ \beta_2 \\ \vdots \\ \beta_m \end{bmatrix}, \quad \text{where} \quad \begin{bmatrix} \beta_1 \\ \beta_2 \\ \vdots \\ \beta_m \end{bmatrix} \sim \mathcal{N}(0, \mathbf{B} \otimes \tilde{\mathbf{I}}_{(p_1+1)(p_2+1)}), \quad (\text{B4})$$

where $\tilde{\mathbf{I}}_{(p_1+1)(p_2+1)}$ is a block diagonal matrix with blocks $\{(1 + \gamma^2)\mathbf{I}_{(p_1+1)}, \mathbf{I}_{p_2}, \mathbf{I}_{p_1 p_2}\}$.

References

1. Hirt C, Amsden A, Cook J. An arbitrary Lagrangian-Eulerian computing method for all flow speeds. *J Comput Phys* 1974; 14(3): 227–253.
2. Liska R, Shashkov M, Vachal P, Wendroff B. Optimization-based synchronized flux-corrected conservative interpolation (remapping) of mass and momentum for arbitrary Lagrangian-Eulerian methods. *J Comput Phys* 2010; 229(5): 1467–1497.
3. Taylor G, Green A. Mechanism of the production of small eddies from large ones. *P Roy Soc Lond A Mat* 1937; 158(895): 499–521. <https://doi.org/10.1098/rspa.1937.0036>, <http://rspa.royalsocietypublishing.org/content/158/895/499>.
4. Knupp P. Winslow smoothing on two-dimensional unstructured meshes. *Eng Comput* 1999; 15: 263–268.
5. Kamm J. Evaluation of the Sedov-von Neumann-Taylor blast wave solution. Tech. Rep. Technical Report LA-UR-00-6055, Los Alamos National Laboratory; The address: 2000.
6. Kucharik M, Shashkov M, Wendroff B. An efficient linearity-and-bound-preserving remapping method. *J Comput Phys* 2003; 188(2): 462–471.
7. Blanchard G, Loubere R. High-Order Conservative Remapping with a posteriori MOOD stabilization on polygonal meshes. Details on how published; 2015. <https://hal.archives-ouvertes.fr/hal-01207156>, the HAL Open Archive, hal-01207156. Accessed January 13, 2016.
8. Burton D, Kenamond M, Morgan N, Carney T, Shashkov M. An intersection based ALE scheme (xALE) for cell centered hydrodynamics (CCH). In: Talk at Multimat 2013, International Conference on Numerical Methods for Multi-Material Fluid Flows. The Organization. ; September 2–6, 2013; San Francisco. LA-UR-13-26756.2.
9. Berndt M, Breil J, Galera S, Kucharik M, Maire P, Shashkov M. Two-step hybrid conservative remapping for multimaterial arbitrary Lagrangian-Eulerian methods. *J Comput Phys* 2011; 230(17): 6664–6687.
10. Kucharik M, Shashkov M. One-step hybrid remapping algorithm for multi-material arbitrary Lagrangian-Eulerian methods. *J Comput Phys* 2012; 231(7): 2851–2864.
11. Breil J, Alcin H, Maire P. A swept intersection-based remapping method for axisymmetric ReALE computation. *Int J Numer Meth Fl* 2015; 77(11): 694–706. Fld.3996.
12. Barth T. Numerical methods for gasdynamic systems on unstructured meshes. In: Kroner D, Rohde C, Ohlberger M., eds. *An Introduction to Recent Developments in Theory and Numerics for Conservation Laws, Proceedings of the International School on Theory and Numerics for Conservation Laws* Lecture Notes in Computational Science and Engineering. Berlin: Springer. 1997. ISBN 3-540-65081-4.
13. Lauritzen P, Erath C, Mittal R. On simplifying ‘incremental remap’-based transport schemes. *J Comput Phys* 2011; 230(22): 7957–7963.
14. Klima M, Kucharik M, Shashkov M. Local error analysis and comparison of the swept- and intersection-based remapping methods. *Commun Comput Phys* 2017; 21(2): 526–558.
15. Dukowicz J, Baumgardner J. Incremental remapping as a transport/advection algorithm. *J Comput Phys* 2000; 160(1): 318–335.
16. Kucharik M, Shashkov M. Flux-based approach for conservative remap of multi-material quantities in 2D arbitrary Lagrangian-Eulerian simulations. In: Fořt J, Fürst J, Halama J, Herbin R, Hubert F., eds. *Finite Volumes for Complex Applications VI Problems & Perspectives*. 1 of *Springer Proceedings in Mathematics*. Springer. 2011 (pp. 623–631).
17. Kucharik M, Shashkov M. Conservative multi-material remap for staggered multi-material arbitrary Lagrangian-Eulerian methods. *J Comput Phys* 2014; 258: 268–304.
18. Loubere R, Shashkov M. A subcell remapping method on staggered polygonal grids for arbitrary-Lagrangian-Eulerian methods. *J Comput Phys* 2005; 209(1): 105–138.

19. Caramana E, Shashkov M. Elimination of artificial grid distortion and hourglass-type motions by means of Lagrangian subzonal masses and pressures. *J Comput Phys* 1998; 142(2): 521–561.
20. Hoch P. An arbitrary Lagrangian-Eulerian strategy to solve compressible fluid flows. Tech. Rep. Technical Report, CEA; The address: 2009. HAL: hal-00366858. <https://hal.archives-ouvertes.fr/docs/00/36/68/58/PDF/ale2d.pdf>. Accessed January 13, 2016.
21. Shashkov M. *Conservative Finite-Difference Methods on General Grids*. Boca Raton, Florida: CRC Press . 1996. ISBN 0-8493-7375-1.
22. Benson D. Computational methods in Lagrangian and Eulerian hydrocodes. *Comput Method Appl M* 1992; 99(2–3): 235–394.
23. Margolin L, Shashkov M. Second-order sign-preserving conservative interpolation (remapping) on general grids. *J Comput Phys* 2003; 184(1): 266–298.
24. Kenamond M, Burton D. Exact intersection remapping of multi-material domain-decomposed polygonal meshes. In: Talk at Multimat 2013, International Conference on Numerical Methods for Multi-Material Fluid Flows. The organization. ; September 2–6, 2013; San Francisco. LA-UR-13-26794.
25. Dukowicz J. Conservative rezoning (remapping) for general quadrilateral meshes. *J Comput Phys* 1984; 54(3): 411–424.
26. Margolin L, Shashkov M. Second-order sign-preserving remapping on general grids. Tech. Rep. Technical Report LA-UR-02-525, Los Alamos National Laboratory; The address: 2002.
27. Mavriplis D. Revisiting the least-squares procedure for gradient reconstruction on unstructured meshes. In: AIAA 2003-3986. 16th AIAA Computational Fluid Dynamics Conference. The organization. ; June 23–26, 2003; Orlando, Florida.
28. Scovazzi G, Love E, Shashkov M. Multi-scale Lagrangian shock hydrodynamics on Q1/P0 finite elements: Theoretical framework and two-dimensional computations. *Comput Method Appl M* 2008; 197(9–12): 1056–1079.